

Theory of Exciton Energy Transfer in Carbon Nanotube Composites

A. H. Davoody,^{1,*} F. Karimi,¹ M. S. Arnold,² and I. Knezevic^{1,†}

¹*Department of Electrical and Computer Engineering,
University of Wisconsin–Madison, Madison, WI 53706-1691, USA*

²*Department of Materials Science and Engineering,
University of Wisconsin–Madison, Madison, WI 53706-1691, USA*

We compute the rate of exciton transfer (ET) between semiconducting single-wall carbon nanotubes (s-SWNTs), mediated by first-order intertube Coulomb coupling. The excitonic states of individual s-SWNTs are calculated by solving the Bethe-Salpeter equation using tight-binding basis functions. The exciton transfer rates between s-SWNTs are computed by treating the direct intertube Coulomb interaction as a perturbation via Fermi's golden rule. Contrary to previous studies, our results show that the ET between perpendicular s-SWNTs is nearly as fast as between parallel tubes. The ET from bright to dark excitonic states is slower by about an order of magnitude than between bright excitonic states. Exciton confinement due to sample inhomogeneity reduces the ET rate between same-chirality bundled SWNTs by two orders of magnitude, but improves the ET rate between bundled SWNTs of dissimilar chiralities by about an order of magnitude. The screening of intertube Coulomb interaction reduces the ET rate, while the screening of intratube Coulomb interactions affects exciton dispersions and wave functions and can improve the ET rate by a factor of two. Moreover, the ET rate between SWNTs increases with increasing temperature. Finally, we show that introducing scattering sources that redistribute excitons between bright and dark states can reduce the ET rate by an order of magnitude.

PACS numbers: 72.20.Pa, 84.60.Rb.,73.63.Nm, 65.80-g

I. INTRODUCTION

Carbon nanotubes (CNTs) are quasi-one-dimensional materials with a unique set of optical and electronic properties [1, 2]. Today, there is considerable interest in semiconducting CNTs as the light-absorbing material in organic solar cells, owing to their tunable band gap, excellent carrier mobility, and chemical stability [3–9]. Improving the efficiency of CNT-based photovoltaic devices is possible through understanding the dynamics of excitons in CNT composites.

While the intratube dynamics of excitons in CNTs have been studied extensively over the past decade [10–18], the intertube exciton dynamics remain relatively unexplored, owing to the difficulties in sample preparation and measurements. It was shown that the fluorescence radiation from bundled single-wall carbon nanotube (SWNT) samples is quenched and the absorption spectra are broadened as a result of Coulomb interaction between SWNTs with various chiralities [19]. The exciton lifetimes in isolated and bundled SWNTs were measured to be on the order of 100 ps and 1 – 2 ps, respectively [15], which underscores the importance of intertube Coulomb interactions in the dynamics of excitons in SWNT aggregates.

There have been a number of measurements of the exciton transfer rates in CNTs, however, the reported rates differ by about two orders of magnitude due to the important role of sample parameters [20]. Pump-probe (PP)

spectroscopy measurements have shown a time constant of about 0.37 ps for the ET process from semiconducting SWNTs to metallic SWNTs [21]. Time-resolved photoluminescence (PL) spectroscopy found the time constants of 0.9 ps and 0.5 ps for the ET from semiconducting SWNTs to metallic and semiconducting SWNTs, respectively [22]. In another study, time-resolved PL spectroscopy has been used to measure the ET between semiconducting SWNTs with a time constant $\tau \approx 70$ ps [23]. Qian *et al.* used spatial high-resolution optical spectroscopy to estimate the time constant of ET between two nonparallel semiconducting SWNTs as $\tau \approx 0.5$ ps [24]. Using PP spectroscopy, the ET time constant between bundled SWNTs was measured to be $\tau \approx 10$ fs for S_{11} excitons [25] [26]. The same study estimated the S_{22} exciton transfer to be very slow due to a momentum mismatch. Another study showed a long-range fast component ($\tau \approx 0.3$ ps), followed by a short-range slow component ($\tau \approx 10$ ps) for the ET process in SWNT films [27]. Grechko *et al.* used a diffusion-based model to explain their measurement of ET process in bundled semiconducting SWNTs samples [28]. They found the time constants of $\tau \sim 0.2 - 0.4$ ps for ET process between bundles of SWNTs and $\tau \approx 7$ ps for ET process inside the SWNT bundles. A more recent study by Mehlenbacher *et al.* revealed ultrafast S_{22} exciton transfer [29].

Many difficulties inherent in experiments can be avoided in a theoretical study of the transfer process. However, to date there have been only two theoretical studies of the exciton transfer rate between semiconducting SWNTs [30, 31]. Wong *et al.* showed that the ideal dipole approximation (known as the Förster the-

* Email: davoody@wisc.edu

† Email: iknezevic@wisc.edu

ory) overestimates the exciton transfer rate by three orders of magnitude. Postupna *et al.* showed that the exciton-phonon coupling could have a prominent effect on the exciton transfer process between (6,4) and (8,4) SWNTs [31]. However, none of these studies account for important parameters, such as the existence of low-lying optically dark excitonic states, chirality and diameter of donor and acceptor CNTs, temperature, confinement of excitons, screening due to surrounding media, and the interaction between various exciton subbands, all of which have been shown, experimentally and theoretically, to play an important role in exciton dynamics in CNTs [11, 12, 27, 32, 33].

In this paper, we present a comprehensive theoretical analysis of Coulomb-mediated intertube exciton dynamics in SWNT composites, in which we pay attention to the complex structure of excitonic dispersions, exciton confinement, screening due to surrounding media, and temperature dependence of the ET rate. We solve the Bethe-Salpeter equation in the GW approximation in the basis of single-particle states obtained from nearest-neighbor tight binding in order to calculate the exciton dispersions and wave functions. We calculate the intertube exciton transfer rate due to Coulomb interaction between SWNTs of different chirality and orientations. For the sake of brevity, in the rest of this paper, we refer to single-wall carbon nanotubes simply as carbon nanotubes unless otherwise is noted.

We show that momentum conservation plays an important role in determining the ET rate between parallel CNTs of different chirality. Moreover, the ET rate dependence on the orientation of donor and acceptor CNT is not as prominent as predicted by previous studies. Our study shows that transfer from S_{22} to S_{11} excitonic states happens with the same rate as the transfer process between same subband states ($S_{11} \rightarrow S_{11}$ and $S_{22} \rightarrow S_{22}$). We show that the exciton confinement could increase or decrease the ET rate depending on the relative orientation and chirality of CNTs. The ET rate increases with increasing temperature. Moreover, the exciton transfer rate drops by about one order of magnitude if exciton scattering between bright and dark excitonic states is allowed. We show that screening of the Coulomb interaction by the surrounding media could enhance the transfer rate by a factor of two if the screening is local, otherwise it decreases the ET rate.

The rest of this paper is organized as follows. In Sec. II, we provide a summary of the physics of excitonic states in CNTs. We review the calculation of exciton wavefunctions by using the tight-binding states as the basis functions. In Sec. III, we introduce the formulation of excitonic energy transfer in CNTs. Section IV shows the ET rate between various excitonic states of CNTs and discusses the effect of the above mentioned parameters. Section V provides a summary of the results. Appendix A shows a detailed derivation of the transfer rates for a completely free exciton.

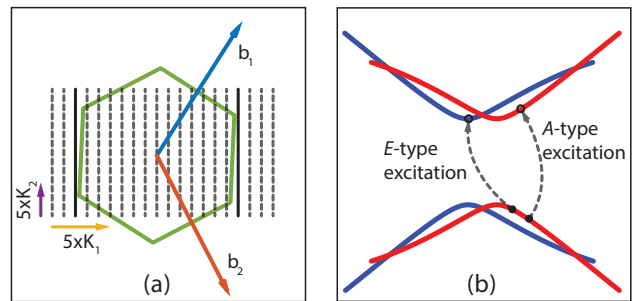


FIG. 1. (a) Graphene Brillouin zone and the cutting lines of CNT with (7,6) chirality. Bold solid cutting lines represent degenerate cutting lines which pass by K and K' points in the graphene Brillouin zone. (b) Schematic of excitation type based on the cutting line of electron and hole.

II. EXCITONS IN CARBON NANOTUBES

In this section, we provide an overview of excitonic states in CNTs. A detailed derivation of these formulas can be found in papers of Rohlfing *et al.* [34] and Jiang *et al.* [35]

A. Single-particle states

For the purpose of calculating the CNT electronic structure, we can consider a CNT as a rolled graphene sheet. Within this picture, a CNT electronic structure is the same as for a graphene sheet. Using the tight binding (TB) method, the CNT wave function is [36]

$$\psi_{\mathbf{a}\mathbf{k}}(\mathbf{r}) = \frac{1}{\sqrt{N_u}} \sum_b \sum_u C_{ab}(\mathbf{k}) e^{i\mathbf{k}\cdot\mathbf{R}_{ub}} \phi(\mathbf{r} - \mathbf{R}_{ub}), \quad (1)$$

where u runs over all the N_u graphene unit cells, $b = A, B$ runs over all the basis atoms in a graphene unit cell, and a is the band index. $\phi(\mathbf{r})$ is the p_z orbital of carbon atom located at the origin. In order to satisfy the azimuthal symmetry of the wavefunction, the wave vector is limited to cutting lines

$$\mathbf{k} = \mu\mathbf{K}_1 + k\mathbf{K}_2/|\mathbf{K}_2|. \quad (2)$$

Here, μ is an integer, determining the cutting line. \mathbf{K}_1 and \mathbf{K}_2 are the reciprocal lattice vectors along the circumferential and axial directions, respectively (Figure 1a). It is noteworthy that there are always two degenerate cutting lines that pass by the two Dirac points (K and K') in the graphene Brillouin zone.

B. Excitonic states

According to the Tamm-Dancoff approximation, the electron-hole excitation (exciton) wave function is a linear combination of free electron-free hole wave functions

[37]

$$|n\rangle = \sum_{\mathbf{k}_c, \mathbf{k}_v} A_n(\mathbf{k}_c, \mathbf{k}_v) \hat{u}^\dagger(\mathbf{k}_c) \hat{v}(\mathbf{k}_v) |\text{GS}\rangle. \quad (3)$$

Here, $A_n(\mathbf{k}_c, \mathbf{k}_v)$ is the expansion coefficient, $\hat{u}^\dagger(\mathbf{k}_c)$ is the creation operator of an electron in the conduction band with wave vector \mathbf{k}_c , and $\hat{v}(\mathbf{k}_v)$ is the annihilation operator of an electron from the valence band with wave vector \mathbf{k}_v . $|\text{GS}\rangle$ is the system ground state, which corresponds to a valence band full and a conduction band empty of electrons. n represents all the quantum numbers. We use the nearest-neighbor tight-binding single-particle wave functions as the basis functions. The expansion coefficients in the exciton wave function and the excitonic eigenenergies are calculated by solving the Bethe-Salpeter (BS) equation

$$[E_c(\mathbf{k}_c) - E_v(\mathbf{k}_v)] A_n(\mathbf{k}_c, \mathbf{k}_v) + \sum_{\mathbf{k}'_c, \mathbf{k}'_v} \mathcal{K}(\mathbf{k}_c, \mathbf{k}_v; \mathbf{k}'_c, \mathbf{k}'_v) A_n(\mathbf{k}'_c, \mathbf{k}'_v) = \Omega_n A_n(\mathbf{k}_c, \mathbf{k}_v), \quad (4)$$

where $E_c(\mathbf{k}_c)$ and $E_v(\mathbf{k}_v)$ are the quasiparticle energies of electrons with wave vectors \mathbf{k}_c and \mathbf{k}_v in the conduction and valence bands, respectively. Ω_n is the exciton energy. \mathcal{K} is the interaction kernel which describes the particle-particle interaction. Using the GW approximation [38], we can divide the interaction kernel into direct and exchange terms

$$\mathcal{K}(\mathbf{k}_c, \mathbf{k}_v; \mathbf{k}'_c, \mathbf{k}'_v) = 2\delta_\alpha \mathcal{K}^x(\mathbf{k}_c, \mathbf{k}_v; \mathbf{k}'_c, \mathbf{k}'_v) - \mathcal{K}^d(\mathbf{k}_c, \mathbf{k}_v; \mathbf{k}'_c, \mathbf{k}'_v), \quad (5a)$$

where the direct interaction depends on the screened Coulomb potential, w ,

$$\mathcal{K}^d(\mathbf{k}_c, \mathbf{k}_v; \mathbf{k}'_c, \mathbf{k}'_v) = W(\mathbf{k}_c, \mathbf{k}'_c; \mathbf{k}_v, \mathbf{k}'_v) = \int d^3\mathbf{r} d^3\mathbf{r}' \psi_{\mathbf{k}'_c}^*(\mathbf{r}') \psi_{\mathbf{k}_c}(\mathbf{r}') w(\mathbf{r}, \mathbf{r}'; \omega = 0) \psi_{\mathbf{k}_v}(\mathbf{r}) \psi_{\mathbf{k}'_v}^*(\mathbf{r}), \quad (5b)$$

and the exchange interaction is calculated using the bare Coulomb potential, v ,

$$\mathcal{K}^x(\mathbf{k}_c, \mathbf{k}_v; \mathbf{k}'_c, \mathbf{k}'_v) = V(\mathbf{k}_c, \mathbf{k}_v; \mathbf{k}'_c, \mathbf{k}'_v) = \int d^3\mathbf{r} d^3\mathbf{r}' \psi_{\mathbf{k}'_c}^*(\mathbf{r}') \psi_{\mathbf{k}_v}(\mathbf{r}') v(\mathbf{r}, \mathbf{r}') \psi_{\mathbf{k}_c}(\mathbf{r}) \psi_{\mathbf{k}'_v}^*(\mathbf{r}). \quad (5c)$$

Here, $\psi_{\mathbf{k}}$ is the quasiparticle (electron or hole) wave function. α is the exciton spin, and $\delta_\alpha = 1$ for singlet excitons ($\alpha = 0$) and $\delta_\alpha = 0$ for triplet excitons ($\alpha = 1$).

The screened Coulomb interaction can be calculated using the random phase approximation [35, 39]

$$W(a_1\mathbf{k}_1, a_2\mathbf{k}_2; a_3\mathbf{k}_3, a_4\mathbf{k}_4) = \frac{V(a_1\mathbf{k}_1, a_2\mathbf{k}_2; a_3\mathbf{k}_3, a_4\mathbf{k}_4)}{\kappa\epsilon(\mathbf{k}_1 - \mathbf{k}_2, \omega = 0)}. \quad (6)$$

Here, a_i represents the conduction or valence band of graphene. κ is the static relative dielectric function, which accounts for the effect of core electrons and the surrounding environment. The effect of π -bond electrons is considered in the relative dielectric function $\epsilon(\mathbf{q}, \omega)$ which is calculated through the Lindhard formula [39].

Using tight-binding single-particle wavefunctions, the interaction kernels are

$$\begin{aligned} \mathcal{K}^d(\mathbf{k}_c, \mathbf{k}_v; \mathbf{k}'_c, \mathbf{k}'_v) &= \delta(\mathbf{k}'_c - \mathbf{k}_c, \mathbf{k}'_v - \mathbf{k}_v) \times \dots \\ &\dots \sum_{b, b'} C_{cb}^*(\mathbf{k}_c) C_{cb}(\mathbf{k}'_c) C_{vb'}(\mathbf{k}_v) C_{vb'}^*(\mathbf{k}'_v) \frac{v_{b, b'}(\mathbf{k}_c - \mathbf{k}'_c)}{\kappa\epsilon(\mathbf{k}_c - \mathbf{k}'_c, 0)}, \\ \mathcal{K}^x(\mathbf{k}_c, \mathbf{k}_v; \mathbf{k}'_c, \mathbf{k}'_v) &= \delta(\mathbf{k}_v - \mathbf{k}_c, \mathbf{k}'_v - \mathbf{k}'_c) \times \dots \\ &\dots \sum_{b, b'} C_{cb}^*(\mathbf{k}_c) C_{vb}(\mathbf{k}_v) C_{cb'}(\mathbf{k}'_c) C_{vb'}^*(\mathbf{k}'_v) v_{b, b'}(\mathbf{k}_c - \mathbf{k}_v), \end{aligned} \quad (7)$$

where $v_{b, b'}(\mathbf{q})$ is the Fourier transform of the overlap matrix between two p_z orbitals

$$\begin{aligned} v_{b, b'}(\mathbf{q}) &= \frac{1}{N_u} \sum_{u'''} e^{i\mathbf{q} \cdot (\mathbf{R}_{u'''} - \mathbf{R}_{0b})} I(\mathbf{R}_{u'''} - \mathbf{R}_{0b}), \\ I(\mathbf{R}_{u'''} - \mathbf{R}_{ub}) &= \int d^3\mathbf{r} d^3\mathbf{r}' |\phi(\mathbf{r} - \mathbf{R}_{ub})|^2 \times \dots \\ &\dots v(|\mathbf{r} - \mathbf{r}'|) |\phi(\mathbf{r}' - \mathbf{R}_{u'''})|^2 \\ &\approx \frac{U}{\sqrt{\left(\frac{4\pi\epsilon_0}{e^2} U |\mathbf{R}_{u'''} - \mathbf{R}_{0b}|\right)^2 + 1}}, \end{aligned} \quad (8)$$

The last expression is the Ohno potential [40], where we take the parameter $U = 11.3$ eV. Note that due to the delta functions in Eq. (7) we can write the interaction kernels in terms of the center-of-mass and relative-motion wave vectors [41]

$$\mathbf{K} = \frac{\mathbf{k}_c - \mathbf{k}_v}{2}, \quad \mathbf{k}_r = \frac{\mathbf{k}_c + \mathbf{k}_v}{2}. \quad (9)$$

Consequently, the center-of-mass wave vector is a good quantum number and we have $n = (s, \mathbf{K})$ in the BS equation. s is the quantum number analogue of the principal quantum in hydrogen atom. The excited state in Eq. (3) is now be written as

$$|s, \mathbf{K}\rangle = \sum_{\mathbf{k}_r} A_s(\mathbf{K}, \mathbf{k}_r) \hat{u}^\dagger(\mathbf{k}_r + \mathbf{K}) \hat{v}(\mathbf{k}_r - \mathbf{K}) |\text{GS}\rangle. \quad (10)$$

Note that both the center-of-mass and relative-motion wave vectors are two-dimensional vectors consisting of two components. (i) A discrete circumferential part, which determines the electron and hole subband indices,

$$\mathcal{M} = (\mu_c - \mu_v)/2, \quad \mu_r = (\mu_c + \mu_v)/2. \quad (11)$$

\mathcal{M} determines the angular momentum of the exciton center of mass. (ii) A continuous part, parallel to the axis of the CNT, which determines how fast they are moving along the CNT,

$$K = (k_c - k_v)/2, \quad k_r = (k_c + k_v)/2. \quad (12)$$

If the exciton center-of-mass angular momentum is zero ($\mathcal{M} = 0$) the exciton is called A -type. In an A -type exciton, the electron and the hole belong to the same cutting lines. On the other hand, if the electron and the hole belong the different cutting lines, the center-of-mass angular momentum is nonzero ($\mathcal{M} \neq 0$) and the exciton is called E -type (See Fig. 1b); E_+ and E_- refer to excitons with positive and negative center-of-mass angular momenta, respectively.

For an A -type exciton ($\mathcal{M} = 0$), it is easy to show that

$$\mathcal{K}^d(\mathbf{k}_r, \mathbf{k}'_r; \mathbf{K}) = \mathcal{K}^d(-\mathbf{k}_r, -\mathbf{k}'_r; \mathbf{K}), \quad (13a)$$

$$\mathcal{K}^x(\mathbf{k}_r, \mathbf{k}'_r; \mathbf{K}) = \mathcal{K}^x(-\mathbf{k}_r, -\mathbf{k}'_r; \mathbf{K}), \quad (13b)$$

$$\mathcal{K}^x(\mathbf{k}_r, \mathbf{k}'_r; \mathbf{K}) = \mathcal{K}^x(\mathbf{k}_r, -\mathbf{k}'_r; \mathbf{K}), \quad (13c)$$

which results in symmetric (A_1) and antisymmetric (A_2) excitons [42]

$$A_1 \text{ exciton} \rightarrow A_s(\mathbf{K}, \mathbf{k}_r) = -A_s(\mathbf{K}, -\mathbf{k}_r), \quad (14)$$

$$A_2 \text{ exciton} \rightarrow A_s(\mathbf{K}, \mathbf{k}_r) = +A_s(\mathbf{K}, -\mathbf{k}_r). \quad (15)$$

The wavefunction of an $A_1(A_2)$ exciton are symmetric (antisymmetric) under C_2 rotation around an axis perpendicular to the unwrapped graphene sheet. Also, the E -type excitons center-of-mass can rotate clockwise (E_+) or anticlockwise (E_-) along the circumference of the CNT. Among the A -type excitons discussed here, only the singlet A_2 exciton is optically active (bright) and the rest are dark excitons (Fig. 2b).

We can calculate the exciton energies for different values of center-of-mass momentum, which yields the exciton dispersion curves. Figure 2 shows the energy dispersions for singlet and triplet excitons, with various symmetries and center-of-mass momentum. Here, it is assumed that the exciton is a result of an S_{11} transition (an electron is excited from the highest valence band to the lowest conduction band).

III. RESONANCE ENERGY TRANSFER: DIRECT INTERACTION

In this section, we calculate the interaction matrix element between excitonic states of two CNTs and the exciton transfer rate due to the interaction (Fig. 3).

The initial and final states of the system are assumed to be those of two noninteracting systems. Here, we assume that the first CNT is the donor CNT which is initially excited, and after the exciton scattering the excitation is transferred to the second, acceptor CNT. Therefore, the exciton initial and final states in this two-CNT system can be denoted by $|I\rangle = |1^*\rangle \otimes |2\rangle$ and $|F\rangle = |1\rangle \otimes |2^*\rangle$,

respectively, where the asterisk denotes an excited state of a given tube. The transfer process is possible through direct and exchange Coulomb interactions between electrons of donor and acceptor CNTs [43, 44]. Figure 4 shows a schematic of the direct and exchange pathways.

The exchange interaction is important for the CNT aggregates with considerable orbital overlaps between the

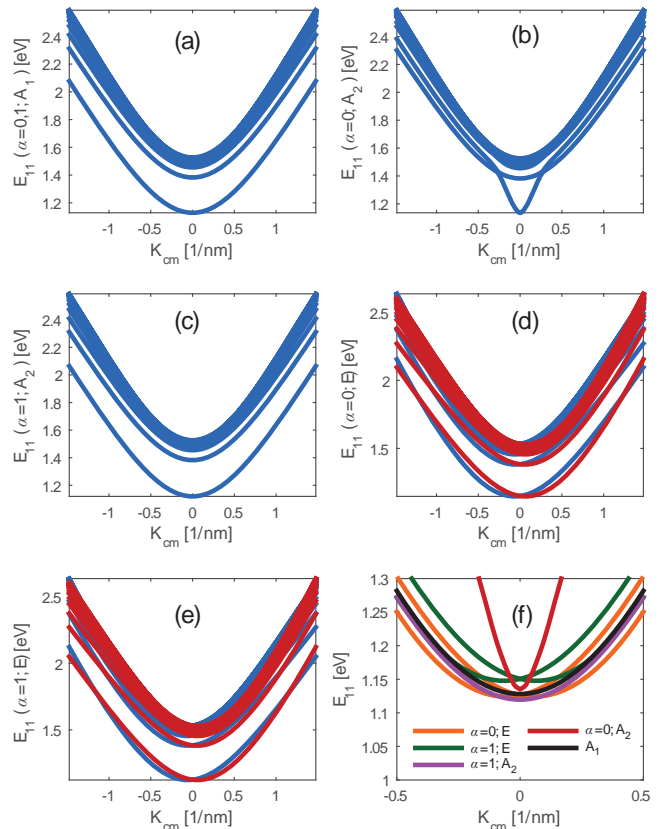


FIG. 2. Energy dispersion of (a) A_1 singlet and triplet exciton, (b) A_2 singlet, (c) A_2 triplet exciton, (d) E type singlet excitons with positive (blue) and negative (red) circumferential momentum, and (e) E type triplet excitons with positive (blue) and negative (red) circumferential momentum for E_{11} transition in (7,5) carbon nanotube. Panel (f) shows a comparison of lowest-subband exciton dispersions for various exciton types. α denotes the exciton spin, so $\alpha = 0$ refers to singlet and $\alpha = 1$ to triplet excitons.

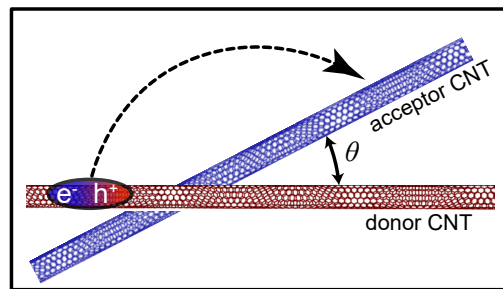


FIG. 3. Geometry of donor (red) and acceptor (blue) carbon nanotubes.

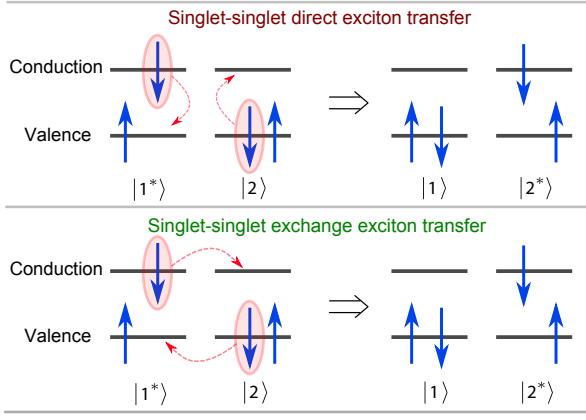


FIG. 4. Schematic of the exciton transfer processes mediated by direct (top) and exchange (bottom) Coulomb interaction.

donor and acceptor systems [43, 44]. When the separation between the donor and acceptor CNTs are larger

than the spatial extent of the p_z orbitals ($< 1 \text{ \AA}$), the direct interaction is dominant. Here, we assume that the donor and acceptor CNTs are not touching (wall-to-wall separation $\approx 2 \text{ \AA}$), hence we only consider the direct Coulomb interaction. The matrix element of the direct interaction is

$$\begin{aligned} \mathcal{M}_d &= \langle s_1, \mathbf{K}_1; \text{GS}_2 | \hat{H}_d | \text{GS}_1; s_2, \mathbf{K}_2 \rangle \\ &= \sum_{\mathbf{k}_{r_1}} \sum_{\mathbf{k}_{r_2}} A_{s_1}^*(\mathbf{K}_1, \mathbf{k}_{r_1}) A_{s_2}(\mathbf{K}_2, \mathbf{k}_{r_2}) \times \cdots \\ &\quad \cdots \langle \mathbf{k}_{v_2}, \mathbf{k}_{c_1} | v(\mathbf{r} - \mathbf{r}') | \mathbf{k}_{c_2}, \mathbf{k}_{v_1} \rangle, \end{aligned} \quad (16)$$

where we have $\mathbf{k}_{c_1} = \mathbf{k}_{r_1} + \mathbf{K}_1$, $\mathbf{k}_{v_1} = \mathbf{k}_{r_1} - \mathbf{K}_1$, $\mathbf{k}_{c_2} = \mathbf{k}_{r_2} + \mathbf{K}_2$, and $\mathbf{k}_{v_2} = \mathbf{k}_{r_2} - \mathbf{K}_2$. The Coulomb potential interacting between the electrons is

$$v(|\mathbf{r} - \mathbf{r}'|) = \frac{e^2}{4\pi\epsilon|\mathbf{r} - \mathbf{r}'|}. \quad (17)$$

Now, we calculate the overlap integral over the free-particle tight-binding wavefunctions

$$\begin{aligned} \mathcal{I}_{\text{TB}} &= \langle \mathbf{k}_{v_2}, \mathbf{k}_{c_1} | v(\mathbf{r} - \mathbf{r}') | \mathbf{k}_{c_2}, \mathbf{k}_{v_1} \rangle = \int d^3\mathbf{r} d^3\mathbf{r}' \psi_{c\mathbf{k}_{c_1}}^*(\mathbf{r}) \psi_{v\mathbf{k}_{v_1}}(\mathbf{r}) v(|\mathbf{r} - \mathbf{r}'|) \psi_{c\mathbf{k}_{c_2}}(\mathbf{r}') \psi_{v\mathbf{k}_{v_2}}^*(\mathbf{r}') \\ &= \frac{1}{N_{u_1} N_{u_2}} \sum_{b_1, b_2, b_3, b_4} C_{cb_1}^*(\mathbf{k}_{c_1}) C_{vb_2}(\mathbf{k}_{v_1}) C_{cb_3}(\mathbf{k}_{c_2}) C_{vb_4}(\mathbf{k}_{v_2}) \sum_{u_1, u_2} \sum_{u_3, u_4} e^{i(-\mathbf{k}_{c_1} \cdot \mathbf{R}_{u_1 b_1} + \mathbf{k}_{v_1} \cdot \mathbf{R}_{u_2 b_2} + \mathbf{k}_{c_2} \cdot \mathbf{R}_{u_3 b_3} - \mathbf{k}_{v_2} \cdot \mathbf{R}_{u_4 b_4})} \times \\ &\quad \cdots \left(\int d^3\mathbf{r} d^3\mathbf{r}' \phi^*(\mathbf{r} - \mathbf{R}_{u_1 b_1}) \phi(\mathbf{r} - \mathbf{R}_{u_2 b_2}) v(|\mathbf{r} - \mathbf{r}'|) \phi^*(\mathbf{r}' - \mathbf{R}_{u_3 b_3}) \phi(\mathbf{r}' - \mathbf{R}_{u_4 b_4}) \right). \end{aligned} \quad (18)$$

Now, we assume that the last integral is nonnegligible only when $u_1 b_1 = u_2 b_2 = ub$ and $u_3 b_3 = u_4 b_4 = u'b'$. Then the overlap integral becomes

$$\begin{aligned} \mathcal{I}_{\text{TB}} &= \frac{1}{N_{u_1} N_{u_2}} \times \cdots \\ &\quad \cdots \sum_{b, b'} C_{cb}^*(\mathbf{k}_{c_1}) C_{vb}(\mathbf{k}_{v_1}) C_{cb'}(\mathbf{k}_{c_2}) C_{vb'}(\mathbf{k}_{v_2}) \times \cdots \\ &\quad \cdots \sum_{u, u'} e^{i[(\mathbf{k}_{v_1} - \mathbf{k}_{c_1}) \cdot \mathbf{R}_{ub} + (\mathbf{k}_{c_2} - \mathbf{k}_{v_2}) \cdot \mathbf{R}_{u'b'}]} \times \cdots \\ &\quad \cdots \int d^3\mathbf{r} d^3\mathbf{r}' |\phi(\mathbf{r} - \mathbf{R}_{ub})|^2 v(|\mathbf{r} - \mathbf{r}'|) |\phi(\mathbf{r}' - \mathbf{R}_{u'b'})|^2. \end{aligned} \quad (19)$$

Considering the small size of atomic orbitals with respect to the separation of the atoms in the two system, we can use a transition monopole approximation (TMA) [30, 45]

$$\int d^3\mathbf{r} d^3\mathbf{r}' |\phi(\mathbf{r} - \mathbf{R}_{ub})|^2 v(|\mathbf{r} - \mathbf{r}'|) |\phi(\mathbf{r}' - \mathbf{R}_{u'b'})|^2 \approx \frac{e^2}{4\pi\epsilon|\mathbf{R}_{ub} - \mathbf{R}_{u'b'}|}. \quad (20)$$

Therefore, we have

$$\begin{aligned} \mathcal{I}_{\text{TB}} &= \frac{e^2}{4\pi\epsilon N_{u_1} N_{u_2}} \times \cdots \\ &\quad \cdots \sum_{b, b'} C_{cb}^*(\mathbf{k}_{c_1}) C_{vb}(\mathbf{k}_{v_1}) C_{cb'}(\mathbf{k}_{c_2}) C_{vb'}(\mathbf{k}_{v_2}) \times \cdots \\ &\quad \cdots \sum_{u, u'} e^{i(-2\mathbf{K}_1 \cdot \mathbf{R}_{ub} + 2\mathbf{K}_2 \cdot \mathbf{R}_{u'b'})} \frac{1}{|\mathbf{R}_{ub} - \mathbf{R}_{u'b'}|}. \end{aligned} \quad (21)$$

Taking the wall-to-wall separation between the tubes large enough that relative positions of basis atoms in donor and acceptor CNTs are not important in calculating the exciton transfer rate, we have

$$\frac{1}{|\mathbf{R}_{ub} - \mathbf{R}_{u'b'}|} \approx \frac{1}{|\mathbf{R}_u - \mathbf{R}_{u'}|}. \quad (22)$$

Therefore, the matrix element is

$$\begin{aligned} \mathcal{I}_{\text{TB}} = & \frac{e^2}{4\pi\epsilon N_{u_1} N_{u_2}} J_\theta(\mathbf{K}_1, \mathbf{K}_2) \left(\sum_{b,b'} C_{cb}^*(\mathbf{k}_{c_1}) \times \cdots \right. \\ & \left. \cdots C_{vb}(\mathbf{k}_{v_1}) C_{cb'}(\mathbf{k}_{c_2}) C_{vb'}^*(\mathbf{k}_{v_2}) e^{i(-2\mathbf{K}_1 \cdot \mathbf{d}_b + 2\mathbf{K}_2 \cdot \mathbf{d}_{b'})} \right) \end{aligned} \quad (23)$$

where we have used $\mathbf{R}_{ub} = \mathbf{R}_u + \mathbf{d}_b$. J_θ is the *geometric part of the matrix element* defined as

$$J_\theta(\mathbf{K}_1, \mathbf{K}_2) = \sum_{u,u'} e^{i(-2\mathbf{K}_1 \cdot \mathbf{R}_u + 2\mathbf{K}_2 \cdot \mathbf{R}_{u'})} \frac{1}{|\mathbf{R}_u - \mathbf{R}_{u'}|}. \quad (24)$$

Therefore, the matrix element for direct Coulomb interaction is

$$\begin{aligned} \mathcal{M}_d = & \frac{e^2 J_\theta(\mathbf{K}_1, \mathbf{K}_2)}{4\pi\epsilon N_{u_1} N_{u_2}} \sum_{\mathbf{k}_{r_1}} \sum_{\mathbf{k}_{r_2}} A_{s_1}^*(\mathbf{K}_1, \mathbf{k}_{r_1}) A_{s_2}(\mathbf{K}_2, \mathbf{k}_{r_2}) \\ & \times \sum_{b,b'} \left(C_{cb}^*(\mathbf{k}_{c_1}) C_{vb}(\mathbf{k}_{v_1}) C_{cb'}(\mathbf{k}_{c_2}) C_{vb'}^*(\mathbf{k}_{v_2}) \times \cdots \right. \\ & \left. \cdots e^{i(-2\mathbf{K}_1 \cdot \mathbf{d}_b + 2\mathbf{K}_2 \cdot \mathbf{d}_{b'})} \right). \end{aligned} \quad (25)$$

Note that, based on the normalization of the exciton wavefunction we have $A_s(\mathbf{K}, \mathbf{k}_r) \propto \frac{1}{\sqrt{N_u}}$, whereas the number of terms in the summation over \mathbf{k}_r increases linearly with N_u . Therefore, in order to extract the size dependence of the matrix element, we introduce a size-independent k -space part of the matrix element

$$\begin{aligned} Q(\mathbf{K}_1, \mathbf{K}_2) = & \frac{e^2}{4\pi\epsilon \sqrt{N_{u_1} N_{u_2}}} \sum_{\mathbf{k}_{r_1}} \sum_{\mathbf{k}_{r_2}} A_{s_1}^*(\mathbf{K}_1, \mathbf{k}_{r_1}) A_{s_2}(\mathbf{K}_2, \mathbf{k}_{r_2}) \\ & \times \sum_{b,b'} C_{cb}^*(\mathbf{k}_{c_1}) C_{vb}(\mathbf{k}_{v_1}) C_{cb'}(\mathbf{k}_{c_2}) C_{vb'}^*(\mathbf{k}_{v_2}) \\ & \times e^{i(-2\mathbf{K}_1 \cdot \mathbf{d}_b + 2\mathbf{K}_2 \cdot \mathbf{d}_{b'})}. \end{aligned} \quad (26)$$

The direct interaction matrix element becomes

$$\mathcal{M}_d = \frac{1}{\sqrt{N_{u_1} N_{u_2}}} J_\theta(\mathbf{K}_1, \mathbf{K}_2) \times Q(\mathbf{K}_1, \mathbf{K}_2). \quad (27)$$

Next, we calculate the exciton scattering rate from donor to acceptor CNTs presented with indices 1 and 2, respectively. If the exciton-phonon and exciton-impurity interaction is stronger than the Coulomb coupling between CNTs, we can assume that the excitons in each CNT have an equilibrium thermal distribution because electron-phonon interaction effectively thermalizes them much faster than the intertube Coulomb-mediated transfer. Therefore, the exciton transfer rate is an average of the exciton scattering rate with the equilibrium thermal distribution. We use Fermi's golden rule to calculate the scattering rate due to direct interaction between CNTs

$$\Gamma_{12} = \frac{2\pi}{\hbar} \sum_{s_1, s_2} \sum_{\mathbf{K}_1, \mathbf{K}_2} \frac{e^{-\beta\Omega_{s_1}}}{\mathcal{Z}} |\mathcal{M}_d|^2 \delta(\Omega_{s_1} - \Omega_{s_2}), \quad (28)$$

where \mathcal{Z} is the partition function

$$\mathcal{Z} = \text{tr}\{e^{-\mathcal{H}/k_B T}\} = \sum_{s_1} \sum_{\mathbf{K}_1} e^{-\beta\Omega_{s_1}}. \quad (29)$$

Assuming the tubes are long enough that we can convert the summation over \mathbf{K}_2 into integration, we get

$$\begin{aligned}
\Gamma_{12} &= \frac{2\pi}{\hbar} \frac{1}{\Delta K_2} \sum_{s_1, s_2} \sum_{\mathbf{K}_1} \sum_{\mathcal{M}_2} \int dK_2 \frac{e^{-\beta\Omega_{s_1}}}{\mathcal{Z}} |\mathcal{M}_d|^2 \delta(\Omega_{s_1} - \Omega_{s_2}) \\
&= \frac{2\pi}{\hbar} \frac{1}{\Delta K_2} \sum_{s_1, s_2} \sum_{\mathbf{K}_1} \sum_{\mathcal{M}_2} \frac{e^{-\beta\Omega_{s_1}}}{\mathcal{Z}} |\mathcal{M}_d|^2 \left(\frac{dK_2}{d\Omega_{s_2}} \right)_{\Omega_{s_1}} \\
&= \frac{2\pi}{\hbar} \frac{1}{N_{u_1} N_{u_2} \Delta K_2} \sum_{s_1, s_2} \sum_{\mathbf{K}_1} \sum_{\mathcal{M}_2} \frac{e^{-\beta\Omega_{s_1}}}{\mathcal{Z}} |J_\theta(\mathbf{K}_1, \mathbf{K}_2) \times Q(\mathbf{K}_1, \mathbf{K}_2)|^2 \left(\frac{dK_2}{d\Omega_{s_2}} \right)_{\Omega_{s_1}}.
\end{aligned} \tag{30}$$

In order to calculate the transfer rate for a limited length CNT, it is better to write this equations in terms of CNT length, therefore, we use the following relations

$$N_{u_1} = \frac{2\pi r_1 L_1}{A_u}, \quad N_{u_2} = \frac{2\pi r_2 L_2}{A_u}, \quad \Delta K_2 = \frac{2\pi}{L_2}. \tag{31}$$

Here, A_u is the area of the graphene unit cell. r_1 and r_2 are the radii of donor and acceptor CNTs, respectively. Therefore, we get

$$\Gamma_{12} = \frac{1}{\hbar L_1} \left(\frac{e^2 A_u^2}{16\pi^3 r_1 r_2} \right)^2 \sum_{s_1, s_2} \sum_{\mathbf{K}_1} \sum_{\mathcal{M}_2} \frac{e^{-\beta\Omega_{s_1}}}{\mathcal{Z}} \left| J_\theta(\mathbf{K}_1, \mathbf{K}_2) \times \tilde{Q}(\mathbf{K}_1, \mathbf{K}_2) \right|^2 \left(\frac{dK_2}{d\Omega_{s_2}} \right)_{\Omega_{s_1}} \tag{32a}$$

where we have defined the renormalized k -part of the matrix element as

$$\tilde{Q}(\mathbf{K}_1, \mathbf{K}_2) = \frac{1}{4\pi\epsilon\sqrt{L_1 L_2}} \sum_{\mathbf{k}_{r_1}} \sum_{\mathbf{k}_{r_2}} A_{s_1}^*(\mathbf{K}_1, \mathbf{k}_{r_1}) A_{s_2}(\mathbf{K}_2, \mathbf{k}_{r_2}) \sum_{b, b'} C_{cb}^*(\mathbf{k}_{c_1}) C_{vb}(\mathbf{k}_{v_1}) C_{cb'}(\mathbf{k}_{c_2}) C_{vb'}^*(\mathbf{k}_{v_2}) e^{i(-2\mathbf{K}_1 \cdot \mathbf{d}_b + 2\mathbf{K}_2 \cdot \mathbf{d}_{b'})}. \tag{32b}$$

IV. RESULTS AND DISCUSSION

In this section, we calculate the exciton transfer rates between four different tube chiralities: (7,5), (7,6), (8,6), and (8,7). The energies of the lowest bright excitonic states in these CNTs are shown in Table I. Figure 5 shows a comparison of the dispersions of optically active S_{11} and S_{22} excitonic states in (7,5) and (8,7) CNTs. We have taken the separation between centers of donor and acceptor CNTs to be 1.2 nm. This distance provides enough wall-to-wall distance ($\approx 2 \text{ \AA}$) between the CNTs under consideration that the exchange Coulomb interactions are negligible.

In this section, we calculate the exciton transfer rates across different combinations of transition subbands (i.e., S_{ii} to S_{jj}). Moreover, we calculate the exciton transfer rate between optically bright and optically dark excitonic states. We report on the dependence of the exciton transfer rate on the angle between the donor and acceptor tubes. Next, we study the effect of exciton confinement on the exciton transfer rate. Furthermore, we show that the exciton thermalization among both dark and bright states can reduce the exciton transfer rate by an order of magnitude. Also, we study the exciton-transfer-rate variation with varying electrostatic screening due to inhomogeneities in the surrounding medium.

Chirality	S_{11} energy [eV]	S_{22} energy [eV]
(7, 5)	1.136	2.08
(7, 6)	1.053	1.974
(8, 6)	1.014	1.849
(8, 7)	0.9004	1.697

TABLE I. Energy of lowest bright excitonic states for selected SWNTs.

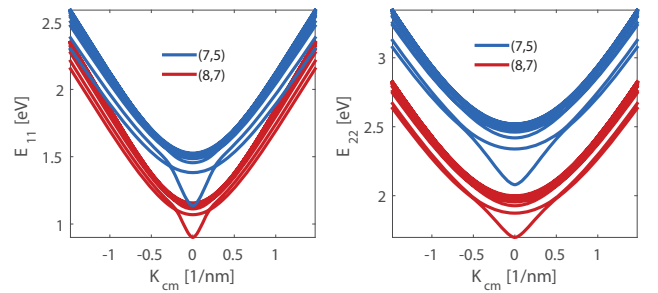


FIG. 5. Comparison of S_{11} (left panel) and S_{22} (right panel) excitonic energy dispersions in (7,5) and (8,7) CNTs.

A. Interband and intraband exciton transfer rates

First, we calculate the exciton transfer rate as a function of the relative angle between donor and acceptor CNTs (angle θ in Fig. 3). Due to the radiative nature of the direct resonance energy transfer (Figure 4), we ex-

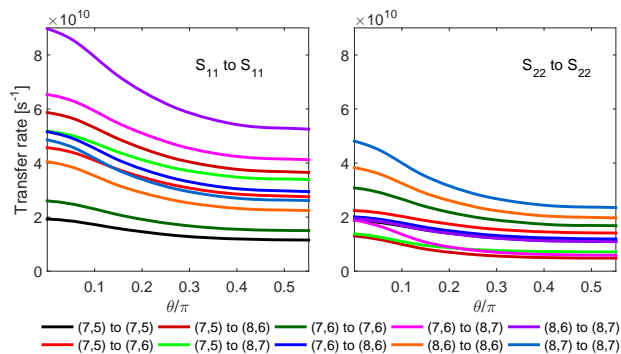


FIG. 6. A_2 exciton transfer rate versus relative angle between donor and acceptor CNTs.

pect the exciton transfer between bright excitonic states to be the dominant transfer pathway. Figure 6 shows the transfer rate of bright excitons (A_2) from donor CNTs with larger band gaps to acceptor CNTs with smaller band gaps (downhill transfer). The uphill exciton transfer process is usually a couple of orders of magnitude smaller, because the excitonic states in the donor tube that can resonate with the acceptor tube states have low exciton population. In Fig. 6, the excitons belong to the same transition subbands in donor and acceptor CNTs (intraband exciton transfer). We assume excitons are confined inside a 10 nm long quantum well, similar to the work by Wong *et al.* [30] We observe a relatively small dependence of ET rate on the relative angle between CNTs. This is in contrast with the prediction by Wong *et al.* [30], who calculated that the transfer rate would drop to zero when the donor and acceptor tubes are perpendicular.

Moreover, exciton transfer rate is slightly higher between S_{11} states than the transfer rate between S_{22} states. This lower transfer rate can be explained from the point of view that the direct resonance energy transfer is a simultaneous process of emission and absorption of a virtual photon by the donor and acceptor system. The S_{22} excitonic states that are in resonance between the donor and acceptor tubes on average have a higher center-of-mass momentum, which yields a lower photon emission rate. [46, 47] The lower rate of electron-photon interaction yields a lower exciton transfer rate between S_{22} states.

Next, we look at the contribution of dark excitonic states in the exciton transfer process. When the separation between donor and acceptor molecules is large compared to the size of each molecule, the traditional Förster theory is applied to calculate the exciton transfer rate. In this case, the transfer process depends on the overlap between the emission and absorption spectra of the donor and acceptor molecules, respectively. Therefore, the dark excitonic states do not contribute in transfer process. However, in the case of exciton transfer between neighboring CNTs, the Förster theory fails as the donor and acceptor molecules are relatively large [30].

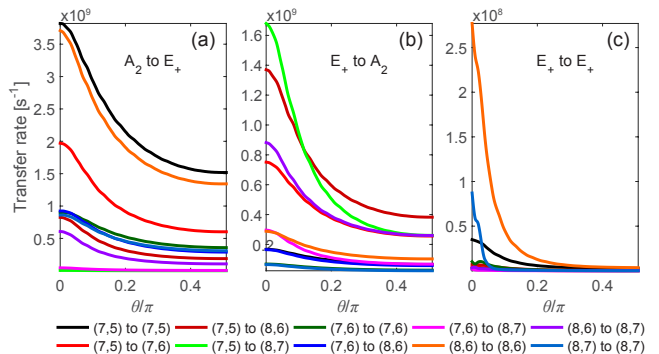


FIG. 7. (a) Transfer rate of A_2 to E_+ excitons as a function of tube orientation. (b) Transfer rate of E_+ to A_2 excitons as a function of tube orientation. (c) Transfer rate of E_+ to E_+ excitons as a function of tube orientation.

Therefore, some dark excitonic states could contribute to the energy transfer process. Figure 7a (7b) shows the downhill exciton rate from bright A_2 (dark E -type) excitonic states to the dark E -type (bright A_2) excitonic states. Transfer rate is about one order of magnitude smaller than the transfer rate between bright excitonic states, owing to the large angular momentum of E -type excitons. Furthermore, exciton transfer from bright to dark excitonic states has a slightly higher rate because of the higher acceptor density of states in the former case. Figure 7c shows the exciton transfer rate between E -type excitonic states (acting as both donor and acceptor state). The transfer rate is two order of magnitude smaller than the transfer rate between bright excitonic states.

We should note that the dark A_1 excitonic states still do not contribute to the exciton transfer process due to symmetry considerations that hold beyond the dipole approximation [35].

Next, we look at the exciton transfer process from the S_{22} excitonic states in the donor tube to the S_{11} excitonic states in the acceptor tube (interband exciton transfer). As we can see in Fig. 8a, the interband energy transfer process occurs with almost the same rate as the intraband exciton transfer process shown in Fig. 6. However, the interband exciton transfer rate is highly dependent on the donor and acceptor tube chirality. The highest transfer rate in Fig. 8a belongs to the exciton transfer from (8,7) to (7,5) SWNTs. As the energy difference between the lowest bright excitonic state (ΔE in Fig. 8b) increases, the exciton transfer rate drops. The slowest transfer rates in Fig. 8a belong to the exciton transfer process from a donor (7,5) tube to acceptor tubes with any other chirality.

In order to better understand the role of different excitonic states in the excitation energy transfer process, we calculated the intra- and interband exciton transfer rates considering only the exciton transfer process between tightly bound excitonic states below the continuum level [48] (white dashed line in Fig. 9b). The calculated

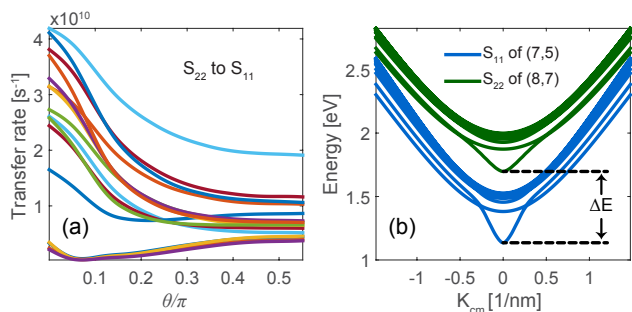


FIG. 8. (a) Transfer rate of bright S_{22} excitonic states to bright S_{11} excitonic states as a function of tube orientation. (b) Excitonic energy dispersions for bright S_{22} excitons in (8,7) and S_{11} excitons in (7,5) SWNTs.

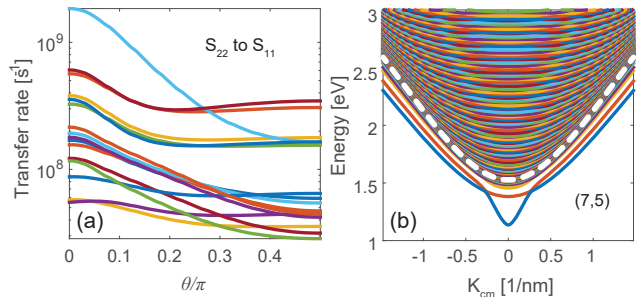


FIG. 9. (a) Exciton transfer rate of bright S_{22} excitonic states to bright S_{11} excitonic states without the contribution of continuum states. (b) Exciton energy dispersions and the continuum states of S_{11} transitions in a (7,5) SWNT. The dashed white curve shows the edge of continuum states.

intraband transfer rate did not change from the case that included both tightly bound excitonic states and the continuum states. However, the interband exciton transfer decreased by at least an order of magnitude (Fig. 9a). We conclude that, although there are many transition states in the continuum region that are resonant between the donor and acceptor states, they do not contribute to the intraband exciton transfer process. However, most of interband exciton transfer process occurs from tightly bound excitonic states to these continuum states.

B. Exciton confinement effect

As a result of inhomogeneities in the surrounding environment and the presence of impurities and defects in the CNT samples, an exciton in a CNT can be confined in one-dimensional quantum wells along the CNT. Here, we study the effect of quantum-well length on the exciton transfer rate. We assume that the confinement does not change the electronic structure of CNTs and the calculated wavefunctions for free (unconfined) excitons are still valid. However, we restrict the extent of the integrals in the geometric part of the matrix elements [Eq. (24)] to the quantum-well length.

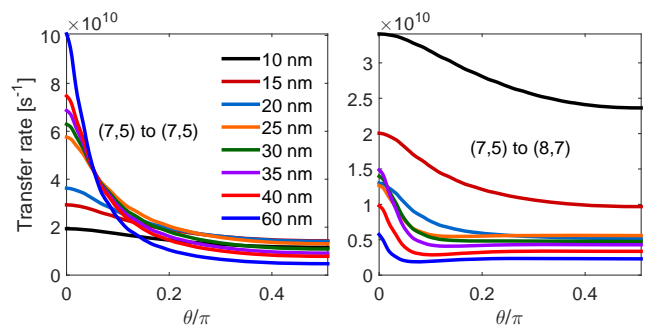


FIG. 10. Exciton transfer rate from bright excitonic states of a donor (7,5) SWNT to the bright excitonic states of (7,5) (panel a) and (8,7) (panel b) acceptor SWNTs. Different colors show the transfer rates of excitons with various confinement lengths.

Figure 10a (10b) shows the exciton transfer rate between bright excitonic states when the donor and acceptor SWNTs have similar (different) chiralities. It is assumed that the confinement lengths in donor and acceptor SWNTs are the same.

When the CNTs are not parallel, the exciton transfer rate drops with increasing confinement length because the average distance between the donor and acceptor systems increases. We can see this length dependence in Eq. (32a). However, in a CNT sample with a constant density of the tubes, the number of available acceptor tubes is proportional to the length of donor CNT as well. Therefore, we can introduce the exciton transfer rate per unit length of donor tube (Fig. 11a). The exciton transfer rate per unit length changes up to a factor of three due to the variation of the geometric part of matrix element [Eq. (32a)]. Nevertheless, the transfer rate stays relatively constant as we go to the limit of free exciton transfer rates. The derivation of an analytical expression for the matrix element and the exciton transfer rate in the case of free excitons in donor and acceptor tubes is discussed in Appendix A.

We observe a different behavior when the donor and acceptor tubes are parallel. This case is particularly important because in many samples the CNTs stick together and form CNT bundles. First, we do not observe a drop in the exciton transfer rate with increasing length of CNTs, as the average distance between the tubes is constant. We can predict this behavior based on the analytical expressions derived in Appendix A. Second, based on the chirality of the donor and acceptor CNTs, the exciton transfer rate follows different trends as the confinement lengths increases. When the confinement length is small, the center-of-mass momentum of initial and final states are not important factors in determining the strength of Coulomb coupling; therefore, there are many states in the acceptor tube that can resonate with the donor-tube excitonic states. However, as the confinement length increases, the contribution from the excitonic states that do not conserve momentum decreases.

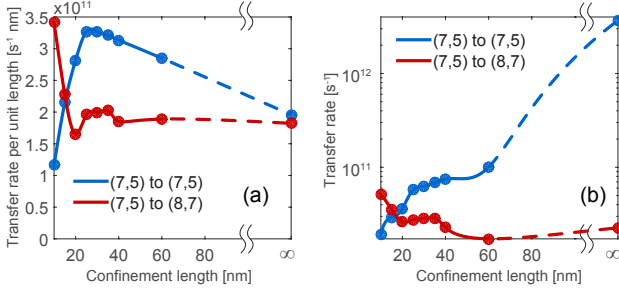


FIG. 11. (a) The exciton transfer rate per unit length between perpendicular donor and acceptor SWNTs as a function of exciton confinement length. (b) The exciton transfer rate between parallel donor and acceptor SWNTs as a function of exciton confinement length.

In the limit of free exciton transfer, only the states that completely conserve the center-of-mass momentum can transfer between the CNTs. When the excitonic energy dispersions in the donor and acceptor tubes are dissimilar (e.g., due to different chiralities), a limited number of states contribute to the exciton transfer process. This results in a decrease of the exciton transfer rate. On the other hand, if the donor and acceptor CNTs have similar dispersion curves, there are many excitonic states that conserve both momentum and energy in donor and acceptor CNTs, which increases the exciton transfer rate by about two orders of magnitude (Fig. 11b).

C. Effect of static screening by surrounding media

In this section, we study another effect of sample inhomogeneity on the exciton transfer process. Like other quasi-one-dimensional nanostructures, the electronic and optical properties of CNTs are influenced by their surrounding media. One of these environmental effects is the screening of electrostatic electron-electron and electron-hole interactions inside a CNT. As we discussed before, the relative permittivity κ in Eq. (6) accounts for the screening due to the surrounding medium and the core ground state electrons in CNTs. As the relative dielectric permittivity, κ , increases, the self-energy due to repulsive electron-electron interaction and the binding energy due to the attractive electron-hole interaction decreases [49]. As shown in Fig. 12a, the net effect is a decrease in exciton energy with increasing permittivity. In the limit of infinite permittivity, we retrieve the noninteracting electron results. Figures 12(b)-(d) show the energy dispersions for bright excitonic states assuming various permittivity for the media. As we expected the binding energy and the number of tightly bound excitonic states decreases with increasing permittivity.

Figure 13a shows the exciton transfer rate between bright excitonic states in (7,5) and (8,7) SWNTs. Overall, the transfer rate decreases with increasing screening from the environment. The main reason is that

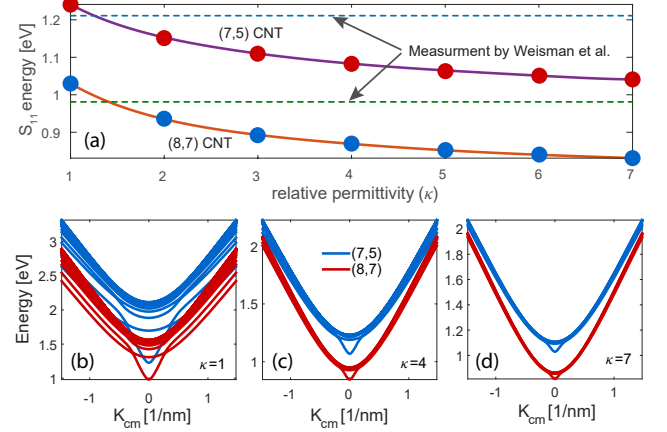


FIG. 12. (a) Lowest transition energies in (7,5) and (8,7) SWNTs as a function of relative permittivity. (b) – (d) Exciton dispersions with various relative dielectric permittivities of the environment.

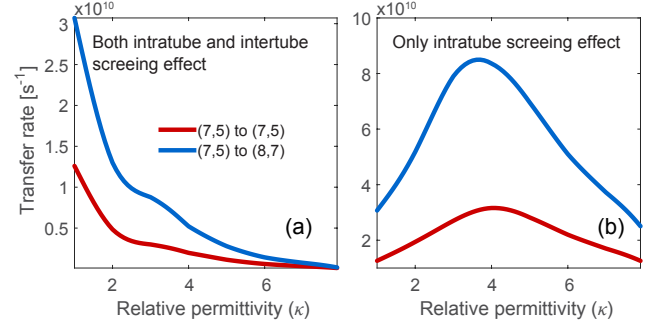


FIG. 13. (a) Lowest transition energies in (7,5) and (8,7) SWNTs as a function of relative permittivity. (b to d) Comparison of exciton dispersion between under various environment dielectric functions.

the electron-electron interaction across the donor and acceptor systems becomes weaker when screening gets stronger. However, the change in exciton transfer rate could be partly from the changes in the exciton dispersion and wavefunction with varying the relative permittivity, κ .

Figure 13b shows the transfer rate when with only considering the changes in the exciton energy and wavefunction. We observe a peak for relative permittivity of $\kappa = 4$. As the exciton dispersion and binding energy change with increasing κ , the number of acceptor states and thus the exciton transfer rate increases (compare Figs. 12 b and c). However, for high permittivities, the excitonic states are more like free-electron free-hole states which have lower photon absorption and emission rates [47]. Therefore, the exciton transfer rate decreases.

D. Interband exciton repopulation

As we discussed earlier, the excitonic states in CNTs are classified as bright and dark states. The former is created via optical stimulation of ground-state electrons and the latter is usually populated through some second-order processes, such as Raman scattering or the scattering of bright excitons into dark excitons by phonons and impurities. So far, we have studied the intrinsic exciton transfer rate from either bright or dark excitonic states. However, if the exciton scattering between bright and dark states is fast enough (compared to the exciton transfer process), the excitons are thermalized among both bright and dark states and we have to consider both in the transfer process.

Figure 14 shows the exciton transfer rate as a function of temperature for the cases of zero and full exciton thermalization in the bright and dark excitonic states. In the presence of exciton thermalization process between bright and dark excitonic states, we observe a twentyfold decrease in the exciton transfer rate. This effect is expected because of the presence of low-lying triplet states and the symmetric singlet states that do not transfer through the direct Coulomb interaction. As the temperature decreases to $T = 0\text{K}$, the excitons only populate these low-lying states and the transfer rate goes to zero. Moreover, the temperature dependence of exciton transfer rate between ideal tubes (i.e., when only bright excitons are populated) decreases with decreasing temperature.

V. CONCLUSION

In summary, we calculated the exciton transfer between four different CNTs. We showed that the exciton transfer rate is weakly dependent on orientation of the tubes. This is in contradiction with the previous studies of the intertube exciton transport. The exciton transfer between bright excitonic states has the highest rate: $2 - 8 \times 10^{10} \text{ s}^{-1}$. The transfer rates between bright and dark states are at least one order of magnitude smaller than the transfer rates between bright excitonic states. The transfer rate between dark excitonic states are negligible. We also looked at the exciton transfer from S_{22} to S_{11} transition energies. We find that the excitons are mainly transferred from tightly bound excitonic states in S_{22} to the continuum level states (equivalent of free electron/free hole states) in S_{11} .

Furthermore, we studied the environmental effects on the exciton transfer rates. We calculated the exciton transfer rate for confined excitons with various confinement lengths. We observed a decrease in the transfer rate between nonparallel tubes, which is due to the increase in the average distance between donor and acceptor systems. By introducing a transfer rate per donor tube length, we showed that the exciton transfer rate is almost independent of the exciton confinement. However,

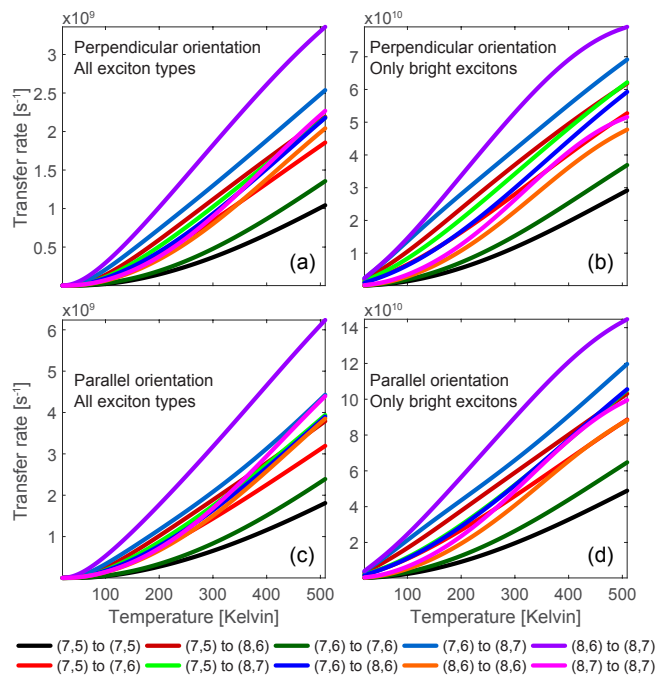


FIG. 14. The exciton transfer rate of confined excitons between SWNTs (a, c) when the excitons are thermalized between both bright and dark excitonic states and (b, d) when only the bright excitonic states are populated. Top (bottom) row shows the transfer rate between perpendicular (parallel) tubes.

exciton transfer between parallel tubes follows a different trend: transfer between same-chirality donor and acceptor tubes is extremely sensitive to confinement and free excitons have the highest transfer rate ($> 10^{12} \text{ s}^{-1}$). The transfer rates between different-chirality tubes are not as sensitive to confinement and only slightly increase with decreasing confinement length. Moreover, we looked at the effect of Coulomb screening due to the surrounding media. The exciton transfer rate decreases with increasing screening. However, the transfer can improve by a factor of two as a result of the changes in exciton wavefunction and energy dispersions.

We showed that the exciton transfer rate increases with rising temperature. This behavior is the opposite of what one would expect based on the emission and absorption spectra of donor and acceptor systems. Also, we showed that the exciton transfer rate drops by about one order of magnitude if excitons are thermalized between bright and dark excitonic states via extrinsic scattering sources.

ACKNOWLEDGMENTS

This work was primarily funded by the U.S. Department of Energy (DOE), Office of Basic Energy Sciences, Division of Materials Sciences and Engineering under DOE Award No. DE-SC0008712. Preliminary efforts (prior to the start of DOE funding) were supported as

part of the University of Wisconsin MRSEC, IRG2 (NSF Grant No. 1121288).

Appendix A: Derivation of exciton transfer rate of free excitons

In this Appendix, we derive the transfer rate of free excitons between two very long CNTs. Let us assume that the CNTs are far enough that, from the point of view of each CNT, the other one looks like a continuum medium, so we can convert the last sum in Eq. (24) to an integral:

$$\sum_{u,u'} e^{i(-2\mathbf{K}_1 \cdot \mathbf{R}_{ub} + 2\mathbf{K}_2 \cdot \mathbf{R}_{u'b'})} \frac{1}{|\mathbf{R}_{ub} - \mathbf{R}_{u'b'}|} \approx \frac{1}{A_u^2} \times \int d^2\mathbf{r} d^2\mathbf{r}' \frac{e^{-2i\mathbf{K}_1 \cdot \mathbf{r}} \times e^{2i\mathbf{K}_2 \cdot \mathbf{r}'}}{|\mathbf{r} - \mathbf{r}'|}. \quad (\text{A1})$$

Assuming that the CNTs are shifted by a center-to-center distance D along the z -axis and they are misoriented by angle θ in the xy plane, the position vectors are

$$\begin{aligned} \mathbf{r} &= x\hat{\mathbf{x}} + r_1 \cos \phi \hat{\mathbf{y}} + r_1 \sin \phi \hat{\mathbf{z}}, \\ \mathbf{r}' &= (x' \cos \theta - r_2 \cos \phi' \sin \theta)\hat{\mathbf{x}} + \dots \\ &\quad \dots (x' \sin \theta + r_2 \cos \phi' \cos \theta)\hat{\mathbf{y}} + (D + r_2 \sin \phi')\hat{\mathbf{z}}. \end{aligned} \quad (\text{A2})$$

$$\begin{aligned} J_\theta(\mathbf{K}_1, \mathbf{K}_2) &= \frac{\pi r_1 r_2}{A_u^2} \int d\phi d\phi' \exp(2i(\mathcal{M}_2 \phi' - \mathcal{M}_1 \phi)) \times \dots \\ &\quad \dots \exp\left(2i \frac{K_1(r_2 \cos \phi' - r_1 \cos \phi \cos \theta) + K_2(r_1 \cos \phi - r_2 \cos \phi' \cos \theta)}{\sin \theta}\right) \times \dots \\ &\quad \dots \frac{\exp(-2 \frac{|D + r_2 \sin \phi' - r_1 \sin \phi|}{\sin \theta} \sqrt{K_2^2 + K_1^2 - 2K_1 K_2 \cos \theta})}{\sqrt{K_2^2 + K_1^2 - 2K_1 K_2 \cos \theta}}. \end{aligned} \quad (\text{A4})$$

Using this relation in Eq. (32a), we can calculate the exciton transfer rate for free excitons. However, the transfer rate between two CNTs goes to zero due to infinitely long donor CNT. However, we can consider the transition rate from a donor CNT to an array of CNTs that are misori-

Therefore, the geometric part of matrix element becomes

Therefore, the last integral would be

$$\begin{aligned} J_\theta(\mathbf{K}_1, \mathbf{K}_2) &= \frac{r_1 r_2}{A_u^2} \int dx dx' d\phi d\phi' \times \dots \\ &\quad \dots e^{-2i(K_1 x + \mathcal{M}_1 \phi) + 2i(K_2 x' + \mathcal{M}_2 \phi')} \times \dots \\ &\quad \dots \left((x' \cos \theta - r_2 \cos \phi' \sin \theta - x)^2 + \dots \right. \\ &\quad \quad \dots (x' \sin \theta + r_2 \cos \phi' \cos \theta - r_1 \cos \phi)^2 + \dots \\ &\quad \quad \left. \dots (D + r_2 \sin \phi' - r_1 \sin \phi)^2 \right)^{-\frac{1}{2}}, \end{aligned} \quad (\text{A3})$$

where r_1 and r_2 are the diameter of carbon nanotube 1 and 2, respectively. If the CNTs are infinitely long, the integrals on x and x' in the geometric part of matrix element can be calculated analytically [50]

ented by angle θ . This is effectively equivalent to having a network of CNTs. The number of acceptor CNTs that the exciton can be transferred to from the initial donor CNT with length L_1 is $N = L_1 \sin \theta / W$, where W is the center-to-center distance in the final array of CNTs. Therefore, the total transfer rate is

$$\kappa_{12}^{tot} = \frac{\sin \theta}{\hbar W} \left(\frac{A_u^2}{4\pi^2 r_1 r_2} \right)^2 \sum_{s_1, s_2} \sum_{\mathbf{K}_1} \sum_{\mathcal{M}_2} \frac{e^{-\beta \Omega_{s_1}}}{\mathcal{Z}} \left| J_\theta(\mathbf{K}_1, \mathbf{K}'_2) \times \tilde{Q}(\mathbf{K}_1, \mathbf{K}_2) \right|^2 \left(\frac{dK_2}{d\Omega_{s_2}} \right)_{\Omega_{s_1}}. \quad (\text{A5})$$

This equation turns out to be divergent at $\theta \rightarrow 0$. This is simply due to the fact that the transfer rate between completely parallel CNTs is length-independent and we

expect the transfer rate from the initial CNT to an infinite number of final CNTs placed at a certain distance becomes infinite. [51]

1. Special case of free exciton transfer between parallel tubes

When the CNTs are very long and parallel to each other, the geometric part of the matrix element yields a Kronecker delta function

$$J_\theta(\mathbf{K}_1, \mathbf{K}_2) = L \times \delta(K_1, K_2) \times C(\mathcal{M}_1, \mathcal{M}_2; K_1), \quad (\text{A6a})$$

$$C(\mathcal{M}_1, \mathcal{M}_2; K_1) = \frac{2r_1 r_2}{A_u^2} \int d\phi d\phi' e^{2i(\mathcal{M}_2 \phi' - \mathcal{M}_1 \phi)} \times \dots \quad (\text{A6b})$$

$$\dots \mathcal{K}_0(|2K_1| \sqrt{(r_1 \sin \phi - r_2 \sin \phi')^2 + (D + r_1 \cos \phi - r_2 \cos \phi')^2}),$$

$L_1 = L_2 = L \rightarrow \infty$ is the length of CNTs. \mathcal{K}_0 is the modified Bessel function of the second kind. Therefore, the matrix element of direct Coulomb interaction becomes

$$\mathcal{M}_d = \frac{A_u^2}{4\pi^2 r_1 r_2} \delta(K_1, K_2) C(\mathcal{M}_1, \mathcal{M}_2; K_1) \times \tilde{Q}(\mathbf{K}_1, \mathbf{K}_2) \quad (\text{A7})$$

Using the conservation of the continuous components of wave vectors \mathbf{K}_1 and \mathbf{K}_2 in the matrix element \mathcal{M}_d , in Eq. 28 we get

$$\begin{aligned} \Gamma_{12} &= \frac{2\pi}{\hbar} \left(\frac{A_u^2}{4\pi^2 r_1 r_2} \right)^2 \sum_{s_1, s_2} \sum_{\mathbf{K}_1} \sum_{\mathcal{M}_2} \frac{e^{-\beta \Omega_{s_1}}}{\mathcal{Z}} \left| C(\mathcal{M}_1, \mathcal{M}_2; K_1) \times \tilde{Q}(\mathbf{K}_1, \mathbf{K}'_2) \right|^2 \delta(\Omega_{s_1} - \Omega'_{s_2}) \\ &= \frac{2\pi}{\hbar} \frac{L}{2\pi} \left(\frac{A_u^2}{4\pi^2 r_1 r_2} \right)^2 \sum_{s_1, s_2} \sum_{\mathcal{M}_1} \sum_{\mathcal{M}_2} \int dK_1 \frac{e^{-\beta \Omega_{s_1}}}{\mathcal{Z}} \left| C(\mathcal{M}_1, \mathcal{M}_2; K_1) \tilde{Q}(\mathbf{K}_1, \mathbf{K}'_2) \right|^2 \delta(\Omega_{s_1} - \Omega'_{s_2}) \quad (\text{A8}) \\ &= \frac{L}{\hbar} \left(\frac{A_u^2}{4\pi^2 r_1 r_2} \right)^2 \sum_{s_1, s_2} \sum_{\mathbf{K}'_1} \sum_{\mathcal{M}_2} \frac{e^{-\beta \Omega_{s_1}}}{\mathcal{Z}} \left| C(\mathcal{M}_1, \mathcal{M}_2; K'_1) \times \tilde{Q}(\mathbf{K}'_1, \mathbf{K}'_2) \right|^2 \left(\frac{dK_1}{d\Omega_{s_1}} \right)_{\Omega'_{s_1}} \end{aligned}$$

The primed quantities in the last relation show the excitonic states in the acceptor CNT that conserve the continuous component of the center-of-mass wave vector, i.e., $K_2 = K_1$. The double primed quantities represent the excitonic states on the donor CNT that conserve both the energy and the continuous part of the center-of-mass momentum in the transfer process, i.e., $\Omega_{s_1}(\mathcal{M}_1, K_1) = \Omega_{s_1}(\mathcal{M}_2, K_1)$. We should note that the final transfer rate is independent of the CNT length as the partition function, \mathcal{Z} , is linearly dependent on the length of the donor CNT and cancels the parameter L in the last equation.

-
- | | |
|--|--|
| <p>[1] D. Jariwala, V. K. Sangwan, L. J. Lauhon, T. J. Marks, and M. C. Hersam, <i>Chem. Soc. Rev.</i> 42, 2824 (2013).</p> <p>[2] M. S. Arnold, J. L. Blackburn, J. J. Crochet, S. K. Doorn, J. G. Duque, A. Mohite, and H. Telg, <i>Phys. Chem. Chem. Phys.</i> 15, 14896 (2013).</p> <p>[3] R. M. Jain, R. Howden, K. Tvrđy, S. Shimizu, A. J. Hilmer, T. P. McNicholas, K. K. Gleason, and M. S. Strano, <i>Adv. Mater.</i> 24, 4436 (2012).</p> <p>[4] D. J. Bindl, M. J. Shea, and M. S. Arnold, <i>Chemical Physics</i> 413, 29 (2013).</p> <p>[5] Y. Ye, D. J. Bindl, R. M. Jacobberger, M.-Y. Wu, S. S. Roy, and M. S. Arnold, <i>Small</i> 10, 3299 (2014).</p> <p>[6] D. J. Bindl, A. S. Brewer, and M. S. Arnold, <i>Nano Res.</i> 4, 1174 (2011).</p> <p>[7] D. J. Bindl, N. S. Safron, and M. S. Arnold, <i>ACS Nano</i> 4, 5657 (2010).</p> <p>[8] M.-H. Ham, G. L. C. Paulus, C. Y. Lee, C. Song,</p> | <p>K. Kalantar-zadeh, W. Choi, J.-H. Han, and M. S. Strano, <i>ACS Nano</i> 4, 6251 (2010).</p> <p>[9] D. J. Bindl, M.-Y. Wu, F. C. Prehn, and M. S. Arnold, <i>Nano Lett.</i> 11, 455 (2011).</p> <p>[10] L. Lüer, S. Hoseinkhani, D. Polli, J. Crochet, and T. Hertel, <i>Nature Phys.</i> 5, 54 (2009).</p> <p>[11] V. Perebeinos, J. Tersoff, and P. Avouris, <i>Nano Letters</i> 5, 2495 (2005).</p> <p>[12] C. D. Spataru, S. Ismail-Beigi, R. B. Capaz, and S. G. Louie, <i>Phys. Rev. Lett.</i> 95, 247402 (2005).</p> <p>[13] K. M. Y. Miyachi, H. Hirori and Y. Kanemitsu, <i>Phys. Rev. B</i> 80, 081410(R) (2009).</p> <p>[14] G. N. Ostojic, S. Zaric, J. Kono, M. S. Strano, V. C. Moore, R. H. Hauge, and R. E. Smalley, <i>Phys. Rev. Lett.</i> 92, 117402 (2004).</p> <p>[15] L. Huang, H. N. Pedrosa, and T. D. Krauss, <i>Phys. Rev. Lett.</i> 93, 017403 (2004).</p> |
|--|--|

- [16] M. W. Graham, J. Chmeliov, Y.-Z. Ma, H. Shinohara, A. A. Green, M. C. Hersam, L. Valkunas, and G. R. Fleming, *J. Phys. Chem. B* **115**, 5201 (2010).
- [17] C. Manzoni, A. Gambetta, E. Menna, M. Meneghetti, G. Lanzani, and G. Cerullo, *Phys. Rev. B* **94**, 207401 (2005).
- [18] A. Hagen, M. Steiner, M. B. Raschke, C. Lienau, T. Hertel, H. Qian, A. J. Meixner, and A. Hartschuh, *Phys. Rev. Lett.* **95**, 197401 (2005).
- [19] M. J. O'Connell, S. M. Bachilo, C. B. Huffman, V. C. Moore, M. S. Strano, E. H. Haroz, K. L. Rialon, P. J. Boul, W. H. Noon, C. Kittrell, J. Ma, R. H. Hauge, R. B. Weisman, and R. E. Smalley, *Science* **297**, 5581 (2002).
- [20] T. Koyama, Y. Miyata, K. Asaka, H. Shinohara, Y. Saito, and A. Nakamura, *J. Phys. Chem. Lett.* **2**, 127 (2010).
- [21] A. Maeda, S. Matsumoto, H. Kishida, T. Takenobu, Y. Iwasa, H. Shimoda, O. Zhou, M. Shiraishi, and H. Okamoto, *J. Phys. Soc. Jpn.* **75**, 043709 (2006).
- [22] T. Koyama, K. Asaka, N. Hikosaka, H. Kishida, Y. Saito, and A. Nakamura, *J. Phys. Chem. Lett.* **2**, 127 (2010).
- [23] S. Berger, C. Voisin, G. Cassabois, C. Delalande, and P. Roussignol, *Nano Lett.* **7**, 398 (2007).
- [24] H. Qian, C. Georgi, N. Anderson, A. A. Green, M. C. Hersam, L. Novotny, and A. Hartschuh, *Nano Letters* **8**, 1363 (2008).
- [25] S_{ij} exciton corresponds to the electron transition from i -th highest valence to the j -th lowest conduction bands.
- [26] L. Lüer, J. Crochet, T. Hertel, G. Cerullo, and G. Lanzani, *ACS Nano* **4**, 4265 (2010).
- [27] R. D. Mehlenbacher, M. Y. Wu, M. Grechko, J. E. Laaser, M. S. Arnold, and M. T. Zanni, *Nano Lett.* **97**, 091905 (2013).
- [28] M. Grechko, Y. Ye, R. D. Mehlenbacher, T. J. McDonough, M. Y. We, R. M. Jacobbreger, M. S. Arnold, and M. T. Zanni, *ACS Nano* **8**, 5383 (2014).
- [29] R. D. Mehlenbacher, T. J. McDonough, M. Grechko, M.-Y. Wu, M. S. Arnold, and M. T. Zanni, *Nature Communications* **6**, 6732 (2015).
- [30] C. Y. Wong, C. Curutchet, S. Tretiak, and G. D. Scholes, *J. Chem. Phys.* **130**, 081104 (2009).
- [31] O. Postupna, H. M. Jaeger, and O. V. Prezhdo, *J. Phys. Chem. Lett.* **5**, 3872 (2014).
- [32] V. Perebeinos, J. Tersoff, and P. Avouris, *Phys. Rev. Lett.* **92**, 257402 (2004).
- [33] A. R. Nugraha, R. Saito, K. Sato, P. T. Araujo, A. Jorio, and M. S. Dresselhaus, *Appl. Phys. Lett.* **13**, 1495 (2013).
- [34] M. Rohlfling and S. G. Louie, *Phys. Rev. B* **62**, 4927 (2000).
- [35] J. Jiang, R. Saito, G. G. Samsonidze, A. Jorio, S. G. Chou, G. Dresselhaus, and M. S. Dresselhaus, *Phys. Rev. B* **75**, 035407 (2007).
- [36] R. Saito, G. Dresselhaus, and M. S. Dresselhaus, *Physical properties of carbon nanotubes*, Vol. 35 (World Scientific, 1998).
- [37] A. Fetter and J. D. Walecka, *Quantum Theory of Many Particle Systems* (McGraw-Hill, San Francisco, 1971) p. 538.
- [38] G. Strinati, *La Rivista del Nuovo Cimento* **11**, 1 (1988).
- [39] N. E. Brener, *Phys. Rev. B* **11**, 1600 (1975).
- [40] K. Ohno, *Theoretica chimica acta* **2**, 219 (1964).
- [41] Note that in the electron-hole picture, the wave vector of excited electron in the valence band is negative of the wave vector of created hole: $\mathbf{k}_h = -\mathbf{k}_v$.
- [42] E. B. Barros, R. B. Capaz, A. Jorio, G. G. Samsonidze, A. G. S. Filho, S. Ismail-Beigi, C. D. Spataru, S. G. Louie, G. Dresselhaus, and M. S. Dresselhaus, *Phys. Rev. B* **73**, 241406(R) (2006).
- [43] G. D. Scholes, *Annu. Rev. Phys. Chem.* **54**, 57 (2003).
- [44] V. May and O. Kühn, *Charge and energy transfer dynamics in molecular systems* (John Wiley & Sons, 2008).
- [45] J. C. Chang, *J. Chem. Phys.* **67**, 3901 (1977).
- [46] C. D. Spataru, S. Ismail-Beigi, L. X. Benedict, and S. G. Louie, *Phys. Rev. Lett.* **92**, 077402 (2004).
- [47] E. Malic, J. Maultzsch, S. Reich, and A. Knorr, *Phys. Rev. B* **82**, 035433 (2010).
- [48] The continuum level is the minimum energy level beyond which the excitonic state can essentially be considered as free electron and free hole states.
- [49] M. S. D. K. S. P. T. Araujo, A. Jorio and R. Saito, *Phys. Rev. Lett.* **103**, 146802 (2009).
- [50] B. M. Project, A. Erdélyi, and H. Bateman, *Tables of Integral Transforms: Based in Part on Notes Left by Harry Bateman and Compiled by the Staff of the Bateman Manuscript Project* (McGraw-Hill, 1954).
- [51] S. K. Lyo, *Phys. Rev. B* **73**, 205322 (2006).